CrossMark

ORIGINALPAPER

In-Situ DRIFT Study of Au–Ir/Ceria Catalysts: Activity and Stability for CO Oxidation

Alejo Aguirre[1] · Celina E. Barrios[1,2] · Antonio Aguilar-Tapia[2] · Rodolfo Zanella[2] ·
Miguel A. Baltanás[1] · Sebastián E. Collins[1]

Abstract Monometallic gold and iridium, and bimetallic gold–iridium on ceria catalysts were synthesized by deposition–precipitation with urea. The activity of these ceria supported catalysts for CO oxidation was: Au–Ir $\gg$ Au > Ir. The bimetallic catalyst was highly active and stable during the carbon monoxide oxidation reaction, showing synergism between both metals. The catalysts were thoroughly characterized chemical and structurally. High-resolution electron microscopy coupled with energy dispersive spectroscopy and X-ray photoelectron spectroscopy showed evidences of iridium–gold intimacy. In situ infrared spectroscopy in the diffuse reflectance mode was used to investigate the reactivity of the active sites. Concentration-modulation excitation spectroscopy allowed selective identification of intermediates and 'spectator' species. CO chemisorbed onto iridium sites (2096, 2060 and 2012 cm^{-1}) was found inactive, whereas carbon monoxide on metallic gold sites (Au^0–CO, 2110 cm^{-1}) exhibited reactivity for CO oxidation. In the bimetallic catalyst, new active sites ($Au^{\delta-}$–CO, 2095 and 2026 cm^{-1}) together with Au^0–CO species were observed, most likely produced by the isolation and stabilization of gold atoms by iridium.

1 Introduction

Catalysts based on gold nanoparticles supported on reducible oxides have been studied intensely because of their high activity to catalyze oxidation reactions at low temperature, particularly CO oxidation [1–4], PROX (selective oxidation of CO in presence of an excess of H_2) [5, 6], or low-temperature water gas shift [7]. More recently, the possibility of removing volatile organic compounds (VOC) by catalytic combustion using gold catalysts has been reported as well. Gold catalysts can perform, for example, the complete oxidation of solvents such as methanol, toluene, propene, benzene and ethyl acetate at low temperature [8–11].

A key factor to improve the activity of gold catalysts is an appropriate choice of the support and the use of proper preparation and activation parameters during synthesis methods. One of the principal issues regarding gold catalysts is their loss of activity during the reaction. In particular, decreased dispersion (sintering) of gold nanoparticles has been alleged as one of the major drawbacks. This lack of stability has hampered their wide use in commercial applications. Many attempts have been made to stabilize gold catalysts by adding to them a second metal. Indeed, the anchoring of the gold particles by addition of a second metal, which decreases their surface mobility, is commonly presented as a viable alternative. Further, the addition of a second metal could change the

✉ Sebastián E. Collins
scollins@santafe-conicet.gov.ar

1 Instituto de Desarrollo Tecnológico para la Industria Química (INTEC) - Universidad Nacional del Litoral and CONICET, Güemes 3450, 3000 Santa Fe, Argentina

2 Centro de Ciencias Aplicadas y Desarrollo Tecnológico, Universidad Nacional Autónoma de México, Circuito Exterior S/N, 04510 Mexico D. F., Mexico

electronic properties of gold particles, or it could change their local atom distribution by the formation of core–shell structures between gold and the added metal.

For these purposes iridium has been used, showing promising results in terms of stability but, also, in activity. Zanella and co-workers studied the catalytic performance of a series of Au–Ir catalysts supported on commercial titania (Evonik P25, a mixture of 80 wt% anatase and 20 wt% rutile) and on pure rutile during the oxidation of CO. They observed that iridium enhanced the activity and the stability of the supported gold nanoparticles [12, 13].

The synergism between gold and iridium in bimetallic systems has also been reported for other catalytic reactions. The enhanced activity of Au–Ir catalysts for the decomposition of dioxins at low temperature was investigated by Haruta and co-workers [14]. This group observed by high-resolution transmission electron microscopy the close interaction between Au nanoparticles and IrO_2 grown epitaxially on a TiO_2 catalyst calcined at 773 K [15]. This interaction was suggested to be responsible for synergism between gold and iridium. Recently, the Ir promotion of TiO_2 supported Au catalysts for selective hydrogenation of cinnamaldehyde has been reported as well [16]. Au–Ir/TiO_2 was found to be fivefold more active than the monometallic gold catalyst for the hydrogenation of cinnamaldehyde to cinnamyl alcohol with high selectivity (S = 83 %).

In this work a ceria-supported gold–iridium was synthetized, characterized and evaluated in the CO oxidation reaction. In situ infrared spectroscopy in the diffuse reflectance (DRIFT) mode, under steady-state reaction conditions and in concentration-modulated experiments was employed to help understand the synergism between gold and iridium.

2 Experimental

2.1 Catalysts

Monometallic gold and iridium, and bimetallic gold–iridium, supported on CeO_2 (Sigma) catalysts were prepared by deposition–precipitation with urea (DPU) [17] using $HAuCl_4 \cdot 3H_2O$ (Sigma) and $IrCl_4 \cdot H_2O$ (Sigma) as metal precursors. For the monometallic catalysts (Au or Ir nominal loading, 3 wt% each), 1 g of ceria was dispersed in an aqueous solution (50 cm^3) containing the metallic precursor (4.2×10^{-3} M) and urea (0.42 M). The suspension was heated to 80 °C for 16 h, under vigorous stirring and in the absence of light, which is known to decompose the gold precursors. Afterwards, the suspension was centrifuged to separate the solid phase, which was then washed with water and resuspended. The new suspension was also

centrifuged, and this procedure was repeated four more times. The solid recovered was dried in vacuum for 2 h at 80 °C.

The bimetallic Au–Ir/CeO_2 catalyst (nominal metals loading: 3 wt% ea.) was prepared by the sequential deposition method reported previously for a rutile catalyst, as follows [12]. Iridium was first deposited on ceria by the DPU method described above. The material was then dried at 80 °C and calcined in air (1 cm^3/min/mg) at 400 °C for 2 h, with a heating rate of 2 °C/min. Then, gold was deposited by the DPU method on the iridium-containing sample, in the dark. After gold deposition, the catalyst precursor was washed, and dried for 2 h at 80 °C. All the catalysts were stored at room temperature under vacuum and in the darkness to prevent any alteration. Prior to use, the catalysts were activated in H_2 (1 cm^3/min/mg) at 400 °C (2 h).

2.2 Characterization

Metal loading was quantified by inductively coupled plasma atomic emission spectroscopy (ICP-AES). Sorption isotherms were measured at liquid nitrogen temperature, in a sorptomatic series 1990 (ThermoQuest). Before experiments all samples were outgassed under dynamic vacuum (base pressure 1.33×10^{-4} Pa) at 120 °C for approximately 4 h. X-ray powder diffraction patterns of the catalysts were measured at room temperature with a Bruker D-8 Advance diffractometer using Cu Kα radiation.

High resolution transmission microscopy (HRTEM) analysis was performed using a Jeol JEM 2010-F (300 kV) equipped with a Z-contrast annular detector. For analyses, the powdered samples were deposited on a copper grid, coated with a porous carbon film. Digital image processing was made using the DigitalMicrograph software, version 3.7.0, Gatan Inc. The histograms of the metal particle sizes were established by the measurement of more than 500 particles obtained by Z-contrast observations.

X-ray photoelectron spectroscopy (XPS) analysis was performed on a multi-technique (SPECS) unit, equipped with a dual X-ray Mg/Al source and a hemispheric analyzer PHOIBOS 150. The spectra were obtained using pass energy of 30 eV, and the Al-Kα X-ray source was operated at 100 W. The working pressure in the analyzing chamber was less than 2×10^{-8} mbar. The binding energies (BE) were referenced to the C (1 s) peak fixed at 284.6 eV. Self-supporting wafers of the catalysts were placed into a heatable sample holder and treated in situ in a pretreatment chamber by reduction in flowing H_2 at 400 °C, followed by outgassing at the same temperature and then cooling to room temperature, after which they were directly transferred without exposure to air to the XPS analysis chamber.

2.3 Catalytic activity

The catalytic activity for CO oxidation [CO(1 %) + O_2(1 %)/He] was evaluated using a continuous plug-flow fixed bed microreactor at atmospheric pressure. For each experiment, 50 mg of powdered catalyst (40/60 mesh) diluted with 100 mg of quartz (100/120 mesh) was placed into the microreactor. The total flow was 100 cm^3/min. The experimental protocols followed heating/cooling cycles. During the first step of the cycle, the catalyst sample was heated from 0 to 200 °C, at a rate of 2 °C/min; then it was kept for 30 min at 200 °C. Finally, the temperature was decreased to room temperature using the same cooling rate. This heating/cooling cycle was repeated twice.

The outlet gas stream was analyzed continuously with an Agilent Technologies 6890 N online gas chromatograph equipped with a FID detector, a methanizer and a HP Plot Q column.

2.4 In situ FTIR Diffuse reflectance

Infrared spectroscopy in DRIFT mode was used to investigate, in situ, the adsorption and dynamic oxidation of CO on the catalysts. The DRIFT cell (Harrick, modified) was mounted inside the sample compartment of the FTIR spectrometer (Thermo-Electron, Nicolet 8700 with a cryogenic MCT detector). The spectrometer bench was continuously purged with dried air (Parker Balston FTIR purge gas generator) to eliminate CO_2 and water vapor contributions to the spectra.

Time-resolved IR spectra were recorded in kinetic and rapid-scan modes at a resolution of 4 cm^{-1}. The background spectrum was collected without catalyst. The amount of catalyst used in the DRIFTS cell was 50 mg, with a bed height of about 5–7 mm. The cell was connected to the feed gas cylinders through low-volume stainless-steel lines. Rapid exchange of the gas composition was performed by switching an electronically actuated flow-through valve (Vici-Valco Instruments), which prevents pressure drop during changes, synchronized with the FTIR spectrometer. The gas flows were set by mass flow controllers. Before CO adsorption and reaction, the catalyst samples were reduced in situ under pure H_2 at 400 °C (2 h), and then cooled down to 35 °C under He flow.

The isothermal reaction of CO oxidation [CO(1 %) + O_2(1 %)/He, 100 cm^3/min] was studied between 35 and 200 °C (steps of 50 °C) on the preactivated catalysts. DRIFT spectra were collected at each temperature once a steady state of the infrared signal was reached (ca. 20 min).

Concentration-modulation excitation spectroscopy (c-MES) experiments were performed at 35 °C, using the same set up already described elsewhere [18]. After recording the background spectrum, a modulation experiment was started by varying the inlet gas composition from CO(1 %)/He to O_2(1 %)/He, while maintaining the same mass flow, using the desired modulation frequency. After allowing at least five modulation periods to adjust the system to the external perturbation the recording of the spectra was started. Spectra were acquired every 3 s, during each c-MES period, using reactants exchange frequencies from 1.7 to 33 mHz. Phase sensitive detection (PSD) analysis of the spectra was performed according to the method developed by Baurecht and Fringeli [19]. More details on the technique can be found in Supplementary Information. For clarity purposes, when indicated, the bands due to the P and R branches of CO in the gas phase were carefully subtracted from the spectra.

3 Results and Discussion

Table 1 summarizes the main morphological and physical characteristics of the support and catalysts used in this study. The surface area of the catalysts was not modified after the deposition of gold and/or iridium onto the ceria support. The measured metal loadings were slightly lower that the nominal amount, but the Au/Ir atomic ratio is close to 1, as their atomic mass is approximately equal.

Figure 1 shows the catalytic performance of the catalysts for the CO oxidation reaction. In order to assess their activity and stability, two consecutive cycles of reaction were performed, by heating and cooling between 0 and 200 °C. The support was only active above 150 °C (see Supplementary Information, Figure S4). The Ir/CeO$_2$ catalyst showed a rather low initial activity to oxidize CO (from 35 °C onwards during the first heating ramp), reaching 100 % conversion at 120 °C (Fig. 1a). Moreover, a noticeably decrease in activity occurred during the second reaction cycle. The T_{50} (that is, the temperature for which 50 % CO conversion was reached), for instance, increased from 90 °C during the first heating ramp to 160 °C in the second one.

Figure 1b shows that the monometallic gold catalyst presented a higher initial activity, reaching a complete CO conversion at approximately 95 °C. The catalytic performance of this catalyst was similar to the one reported for other gold-ceria catalysts under similar reaction conditions [20]. A closer inspection of the evolution of the conversion during the reaction cycles shows that some deactivation took place, though (viz., T_{50} increased from 34 to 41 °C).

The bimetallic Au–Ir/CeO$_2$ catalyst presented the highest activity during the first ramp, showing a 10 % CO

Table 1 Main characteristics of the catalyst and T_{50} values for CO oxidation

Catalyst	Metal loading[a] (wt%)		S_{BET} (m²/g)	Average particle size (nm)[b]	T_{50} CO oxidation (°C)			
	Au	Ir			Heating 1	Cooling 1	Heating 2	Cooling 2
Ir/CeO₂	–	2.5	63	1.0	90	151	151	163
Au/CeO₂	2.9	–	61	1.7	34	39	37	41
Au–Ir/CeO₂	2.5	2.5	62	1.6	20	14	14	14
CeO₂	–	–	62	–	310	–	–	–

[a] Determined by ICP

[b] Determined by STEM-HAADF

conversion already at 0 °C, reaching the complete conversion of CO at 50 °C. Noticeably, during the second cycle the catalyst was more active, and kept stability as well. The activity towards CO oxidation remained remarkably high, with of T_{50} of only 14 °C.

Summarizing, for CO oxidation, the light-off curves for Au–Ir/CeO₂ shifted to lower temperature with respect to either of the monometallic catalysts. Not only the relative reactivity of these ceria supported catalysts was: Au–Ir ≫ Au > Ir but, furthermore, the mass specific activity of the bimetallic Au–Ir catalyst was higher, as indicated in the last two columns of Table 1. This behavior suggests an active interaction between Au and Ir, as it is discussed below.

STEM-HAADF and HRTEM images of the metals supported on ceria revealed that the nanoparticles are homogeneously distributed on the support; their average size is approximately 1.0 nm for Ir and 1.5 nm for Au and Au–Ir. Histograms of the metal particle size distribution and representative HAADF images are presented in Supplementary Information. X-Ray Diffraction patterns were recorded from the activated catalysts (see Figure S4 in Supplementary Information). Only peaks due to the fluorite-type structure of CeO₂ are present, in agreement with the TEM results, which indicate that mostly small particles with diameters below 3.5 nm were present in these materials. These observations are in agreement with numerous contemporary data, where the method employed here to synthesize gold particles led to nanometer sizes. The nanostructural and nanoanalytical analysis suggests a close interaction between gold and iridium. Metal particles located on convex surfaces of the support were selected for chemical analysis by X-ray energy-dispersive spectroscopy (X-EDS). In particular, spot spectrum measurements were carried out through these particles as shown in Fig. 2. The X-EDS spectrum presented in the inset of Fig. 2 clearly shows that iridium and gold are present in the same nanoparticles.

An XPS study was carried out on the catalysts H₂-reduced in situ at 400 °C. Figure 3 shows the XPS spectra in

the gold and iridium regions. The XPS peaks in the gold 4f region were fitted with Doniach–Sunjic-type curves [3], while a conventional Gaussian–Lorentzian fit was used in the iridium 4f case. In both the monometallic and bimetallic catalysts the characteristic Au $4f_{7/2}$ signal was found at 82.9 eV (Fig. 3a). The position of that signal, usually assigned to small gold particles in the metallic state on reducible oxides, was slightly lower than for bulk gold [3, 21, 22]. The full-width-half-maximum (FWHM) of the Au $4f_{7/2}$ peak is also shown in the figure. The narrow FWHM value (1.5 eV) indicates the presence of only metallic Au in both catalysts.

The monometallic Ir/CeO₂ catalyst presented signals in the 4f region corresponding to metallic Ir particles, $4f_{7/2}$ at 60.2 eV and $4f_{5/2}$ at 63.2 eV [23, 24]. The signals for iridium oxide are almost 2 eV higher (Ir²⁺: $4f_{7/2}$ at 62 eV and $4f_{5/2}$ at 64–65 eV) [25], which allows discarding the presence of oxidized species altogether. The position of the Ir peaks in our catalysts is similar to that reported for iridium supported catalyst on TiO₂ [16, 26, 27].

The bimetallic Au–Ir/CeO₂ catalyst showed XPS signals of iridium in the metallic state. The FWHMs of the Ir peaks were identical to the ones of the monometallic catalyst (Fig. 3b), suggesting that the same chemical species are involved. However, a slight shift to lower BE (0.6 eV) was observed, which suggests some electronic interaction between the Ir and Au atoms, as it will be discussed later.

To help understand the superior catalytic activity of the bimetallic catalyst, a characterization by dynamic CO adsorption using DRIFTS was carried out. Figure 4 shows the spectra taken for the reduced catalysts, collected under steady state flow of CO(1 %)/He to the cell at 35 °C.

In the Au/CeO₂ catalyst, absorption bands at 2107 and 2050 cm⁻¹ were detected and assigned to CO adsorbed on neutral (Au⁰) and on partially negatively charged (Au^δ⁻) gold sites, respectively [28–30]. The origin of negatively charged gold sites on supported gold catalysts has been interpreted as a charge transfer from color centers (oxygen vacancies) on the reduced oxide surface to the gold clusters. The electron transfer from partially reduced oxides,
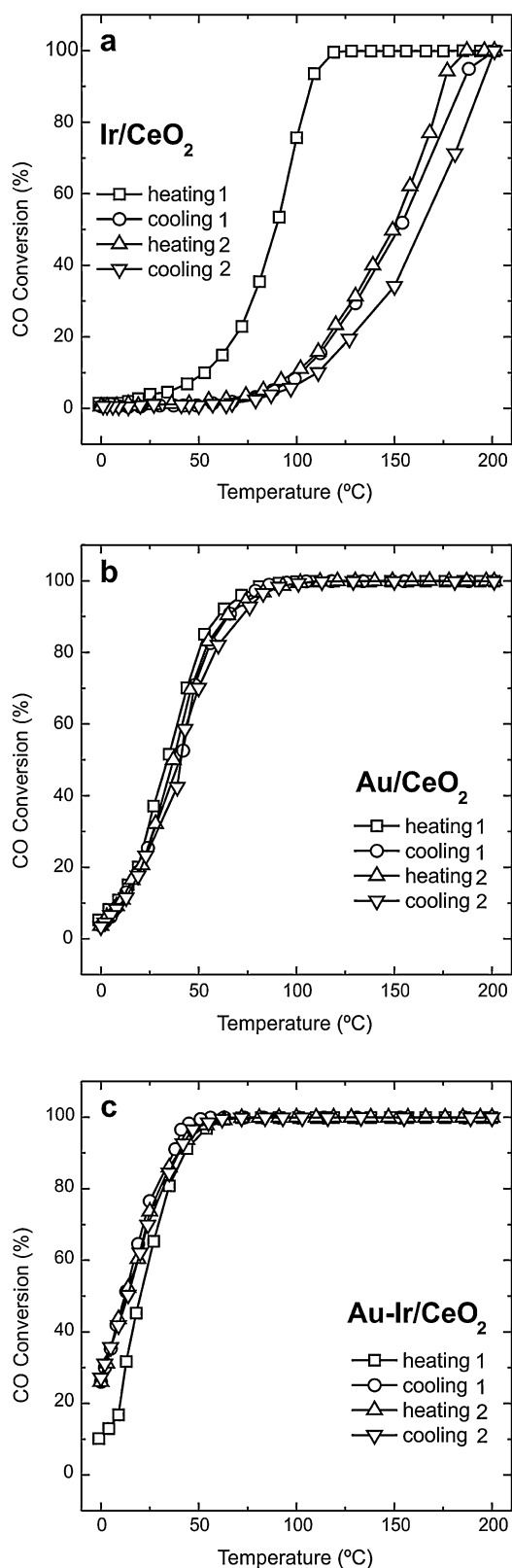
Fig. 1 Evolution of the CO conversion on the Ir/CeO$_2$ (**a**), Au/CeO$_2$ (**b**), and Au–Ir/CeO$_2$ (**c**) catalysts during heating and cooling cycles. Reaction conditions: CO(1 %) + O$_2$(1 %)/He, total flow = 100 cm^3/min, 50 mg of catalyst
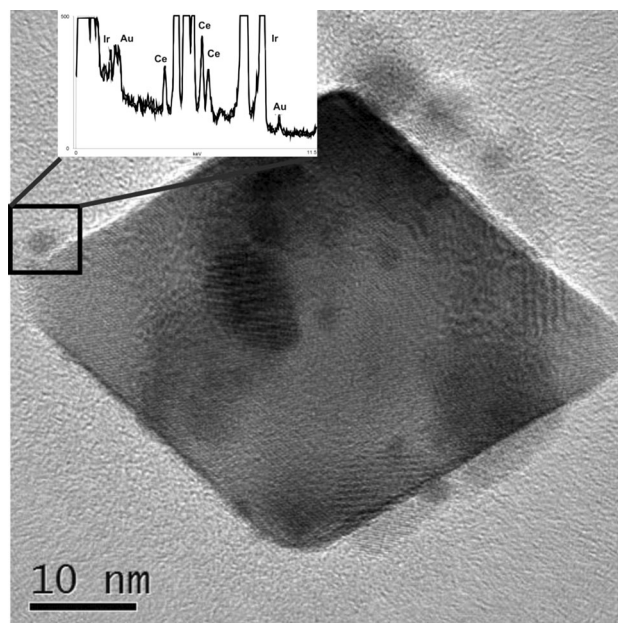

Fig. 2 Representative HRTEM image of the Au–Ir/CeO$_2$ catalyst. *Inset* X-EDS spectrum of a selected nanoparticle, showing the presence of joint gold and iridium

such as TiO$_2$ or MgO to gold atoms, gold clusters or gold films has been corroborated both experimental and theoretically [31–33]. Yet, some controversy still remains in the literature, because low frequency IR bands have been also assigned to chemisorbed CO on non-reducible oxides such as Au/SiO$_2$ [34] and Au/Al$_2$O$_3$ [35].

After adsorption of CO on the Ir/CeO$_2$ catalyst, the IR spectrum exhibited two overlapped peaks at 2080 and 2060 cm^{-1}, and a broad band at 1990 cm^{-1}. Carbon monoxide adsorbed on iridium single crystals presents a single infrared peak in the range 2000–2100 cm^{-1}, assigned to a linear CO species (on-top site) [36–39]. Solymosi et al. [40] studied the adsorption of CO on a reduced Ir/Al$_2$O$_3$ catalyst. The authors assigned a band at 2080–2050 cm^{-1} to Ir^0–CO species and a set of two bands at 2107–2090 and 2040–2010 cm^{-1} to the symmetric and antisymmetric modes, respectively, of Ir$^+$(CO)$_2$ dicarbonyl species. On Ir-ZSM-5, narrow bands at 2182, 2099, and 2074 cm^{-1} were assigned to polycarbonyls, e.g., Ir$^+$(CO)$_3$ [41]. Bianchi and co-workers investigated the adsorption of CO on reduced Ir/Al$_2$O$_3$ and reported a strong IR band at 2044 cm^{-1} associated with two weak shoulders at 2080 and 2000 cm^{-1}. The main IR band was ascribed to linear CO species and the others to geminal species, Ir(CO)$_2$.

The deconvoluted bands registered in our CeO$_2$-supported catalysts are broad and asymmetric, which is suggestive of the presence of somewhat broad distributions of particles sizes, as shown by TEM (see Supplementary Information). Due to the strong reducing
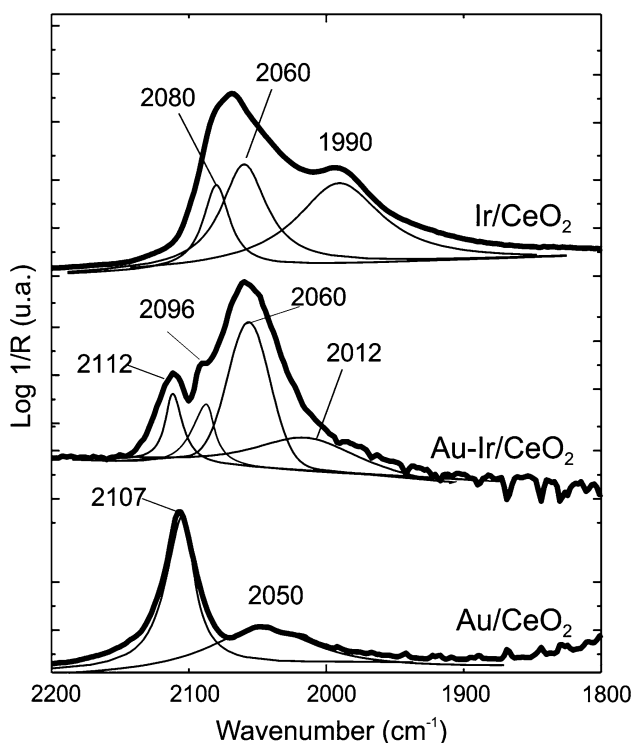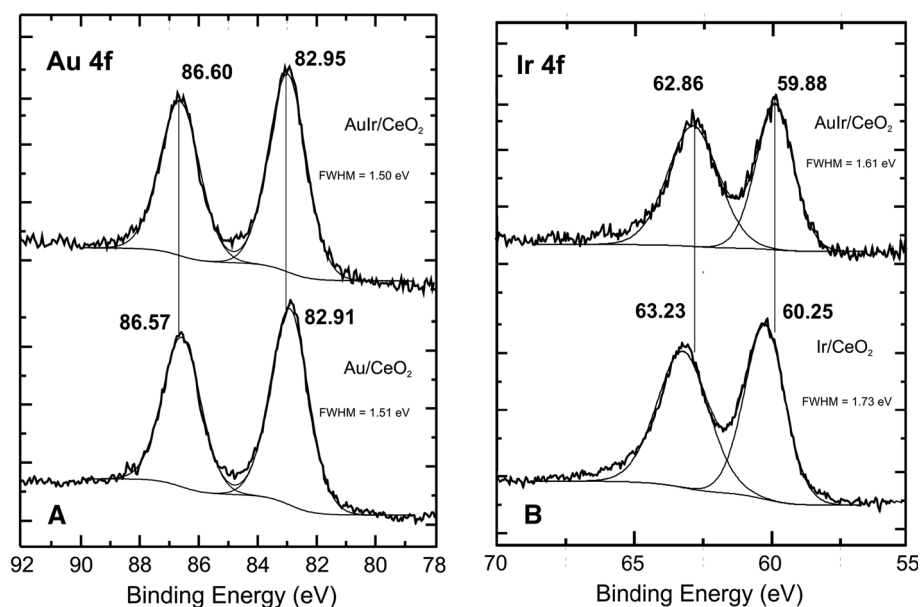
Fig. 4 DRIFT spectra of CO adsorbed on Ir/CeO$_2$, Au–Ir/CeO$_2$ and Au/CeO$_2$ under flowing of CO(1 %)/He at 35 °C (the signals from the gas phase CO were subtracted from the spectra)

treatment applied to the catalysts (H$_2$, 400 °C, 2 h), these IR bands are mainly assigned to CO on metallic Ir sites. Then, the strong band at ca. 2060 cm^{-1} was assigned to linearly adsorbed CO species on low coordination Ir^0 sites, while the features at 2080 and 1990 cm^{-1} were tentatively assigned to dicarbonyl, Ir(CO)$_2$, species,

although we could not disregard, also, a contribution from bridged CO species [16, 42].

Noteworthy, the DRIFT spectrum of adsorbed CO on the bimetallic catalyst was not a linear combination of the monometallic ones. The characteristic feature due to Au^0–CO species appeared at 2112 cm^{-1}. Other peaks could be resolved at 2096, 2060 and 2012 cm^{-1}. The shoulder at 2096 cm^{-1} can be assigned to gold sites in low coordination, due to their isolation by iridium atoms, in a cluster or nanoparticle, or to partially negatively charged sites in interaction with the support, as reported before on reduced Au/CeZrO$_2$ [43]. Finally, the bands at 2060 and 2012 cm^{-1} can be assigned to iridium sites (mainly based on their lack of reactivity, as it will be shown next). The position and shape of these bands was different from those registered on the monometallic catalyst. This could be due to an electronic perturbation/change of the iridium sites as a consequence of the contact with gold, as it was shown in the XPS spectra (Fig. 3). The 'persistence' of the 2060 cm^{-1} IR band in the bimetallic catalyst suggests that some iridium particles still remain apart from the gold crystallites onto the CeO$_2$ surface in this material.

Next, in situ DRIFT spectra were acquired during stepwise CO oxidation at increasing temperatures on the investigated catalysts, by switching the gas flow from CO(1 %)/He to a diluted CO(1 %) + O$_2$(1 %)/He reaction mixture (Fig. 5). The Infrared signals due to CO adsorbed on iridium in the Ir/CeO$_2$ catalyst only showed small changes with temperature. The high heat of adsorption of CO on Ir sites (E$_0$ = 225 kJ/mol and E$_1$ = 115 kJ/mol) is consistent with the high coverage observed up to 200 °C, the maximum temperature used in this work [44]. Conversely, for the monometallic Au/CeO$_2$ catalyst only the
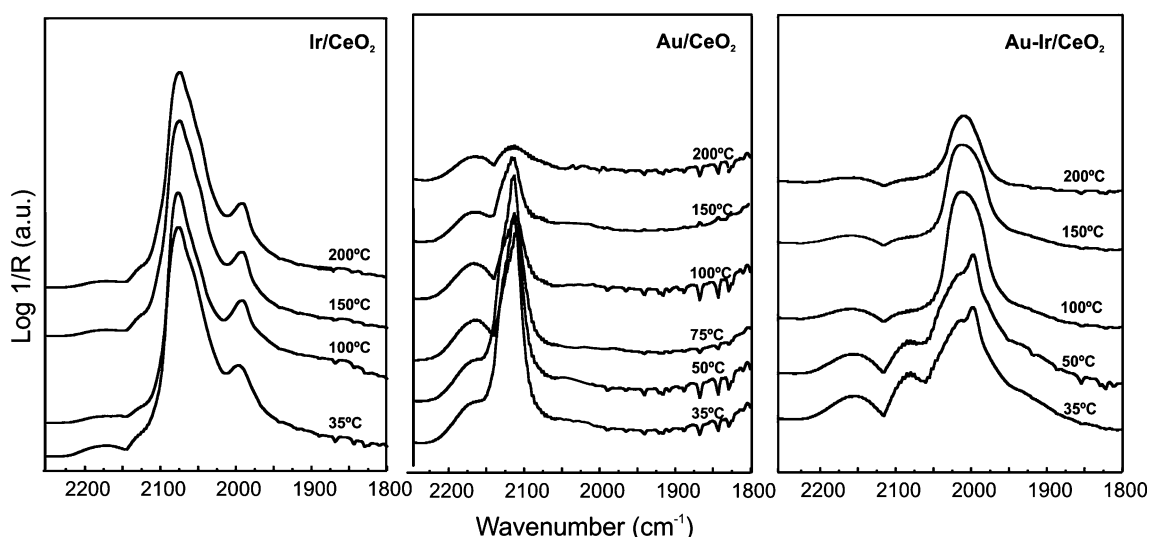
Fig. 5 In situ DRIFT spectra during CO oxidation at increasing temperatures (20 min at each temperature) on the Ir/CeO$_2$, Au/CeO$_2$, and Au–Ir/CeO$_2$ catalysts. Reaction conditions: CO(1 %) + O$_2$(1 %)/He, total flow = 100 cm^3/min, 50 mg of catalyst

band at 2110 cm^{-1} remained after changing the gas flow from CO(1 %)/He to the reaction mixture at 35 °C. This peak lost intensity upon heating, at the same time that the CO conversion increased (see Fig. 1).

The spectrum acquired after switching from CO(1 %)/He to reaction mixture [CO(1 %) + O$_2$(1 %)/He] on the Au–Ir/CeO$_2$ catalyst showed the same bands assigned previously to CO adsorbed on gold and iridium sites. Upon heating, the bands of CO on Au (2107 and 2090 cm^{-1}) diminished, while the one pertaining to CO on iridium at 2040 cm^{-1} remained unchanged, although a change in its shape is observed.

It is clear that obtaining kinetically relevant information on the reactivity of the adsorbed species from spectra collected under steady state, even employing different temperatures, is very difficult. Particularly, it is almost impossible to distinguish intermediates from spectators. Therefore, c-MES experiments were performed to investigate the dynamics of the reactivity of the CO adsorbed species. Figure 6a shows the time-domain spectra during a complete period, 60 s, after exchanging from CO(1 %)/He to O$_2$(1 %)/He on the Ir/CeO$_2$ catalyst at 35 °C. As previously shown, the catalytic activity of the monometallic iridium catalyst at this temperature was very low (Fig. 1a) and, therefore, almost no change in the CO absorption bands was observed. Consequently, the phase-domain spectra, after PSD demodulation, presented in Fig. 6b show only the change in signals from CO in the gas phase.

Figures 7a and b show the time-domain and phase-domain spectra for the monometallic Au/CeO$_2$ catalyst during the c-MES experiment. The signal from adsorbed CO on metallic gold sites (2110 cm^{-1}) was clearly affected by the periodic exchange of reactants. Additionally, the production of
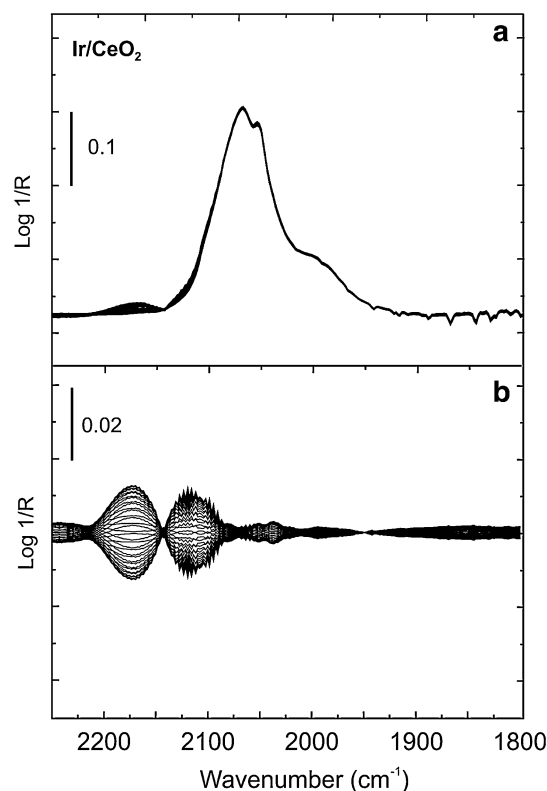
Fig. 6 a Time-domain DRIFT spectra during a c-MES cycle of CO(1 %)/He switched to O$_2$(1 %)/He over Ir/CeO$_2$ (100 cm^3/min, 35 °C, ω = 8.33 mHz); **b** Phase-domain spectra after PSD demodulation
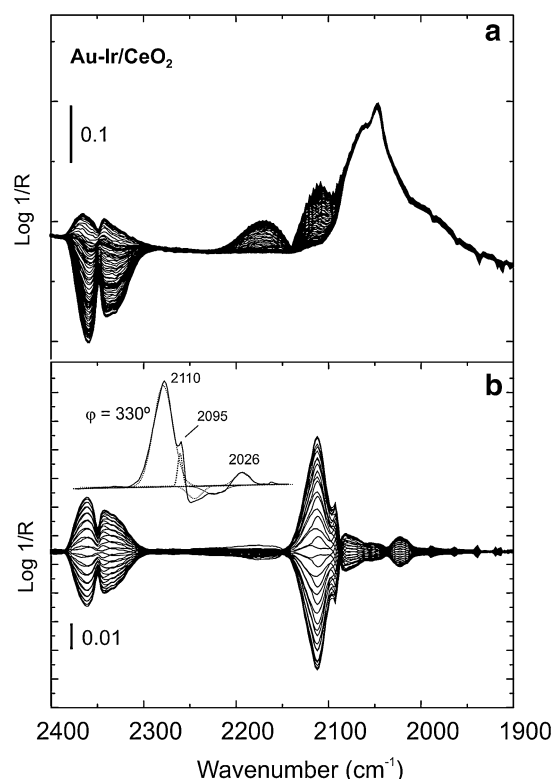
CO$_2$ (2350 cm^{-1}) in the gas phase was observed (not shown). Notably, the bands at low frequency assigned to Au$^{\delta-}$–CO species were not present after exposure to the reaction mixture. This clearly shows that Au–CO are the active species in the
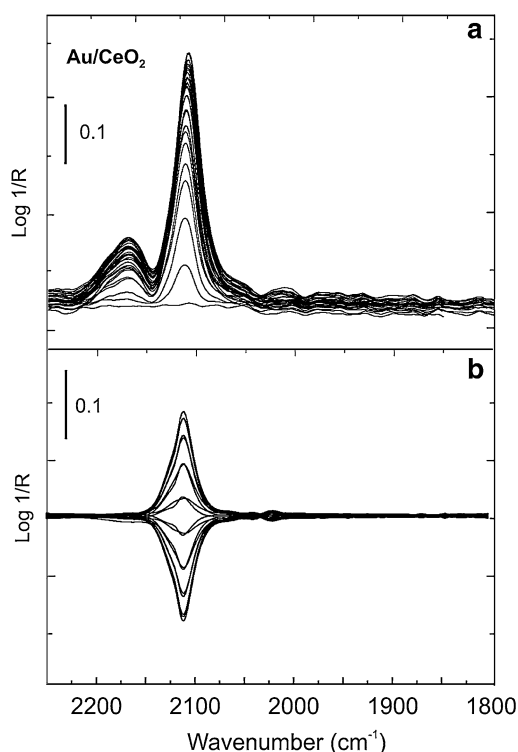
Fig. 7 a Time-domain DRIFT spectra during a c-MES cycle of CO(1 %)/He switched to O₂(1 %)/He over Au/CeO₂ (100 cm³/min, 35 °C, ω = 8.33 mHz) **b** Phase-domain spectra after PSD demodulation

Fig. 8 a Time-domain DRIFT spectra during a c-MES cycle of CO(1 %)/He switched to O₂(1 %)/He over Au–Ir/CeO₂ (100 cm³/min, 35 °C, ω = 8.33 mHz). **b** Phase-domain spectra after PSD demodulation

oxidation of CO on this catalyst, as previously reported for other supported gold materials [30, 45, 46].

In the bimetallic Au–Ir/CeO₂, the most active and stable catalyst, infrared results are more complex to interpret. As seen in Fig. 8a, the time-domain spectra showed a combination of bands, most of which remained constant upon switching the reactants. However, after a PSD analysis, the phase-domain spectra in Fig. 8b allow discerning which signals were affected by the perturbation (note again that for clarity the CO gas bands were subtracted from the spectra). In this case, it can be appreciated that the signals assigned to Ir sites at ca. 2060 cm⁻¹ remained constant, that is, the Ir–CO species were not oxidized and—therefore—are mere spectators of the reaction at this temperature. This last observation supports the previous assignment of this band (Fig. 4). Conversely, as in the monometallic gold system, the Au⁰–CO species (at 2110 cm⁻¹) participated in the reaction. Additionally, new bands were observed at 2095 cm⁻¹ (shoulder) and at 2026 cm⁻¹, which are synchronous with the production of CO₂(g). These last peaks might be assigned to low-coordination and/or negatively charged gold sites (see inset in Fig. 8b). An additional c-MES experiment was carried out, in which the reaction mixture CO(1 %) + O₂(1 %)/He was periodically switched

to pure He. Figures 9a and b show that the evolution of the signals at 2110, 2095 and 2026 cm⁻¹ were then similar than before. Analogous results were obtained performing a c-MES experiment on the Au–Ir/CeO₂ catalyst at 80 °C (see Figure S6 in Supplementary Information).

Goodman et al. showed that gold films (mono- and bilayer structures) grown on reduced TiO₂ exhibited very high activity in CO oxidation [47, 48]. This observation allowed them to conclude that negatively charged gold species play a major role in the reaction. About similar conclusions were drawn from studies carried out on powdered MgO- and CeO₂-supported gold particles catalysts [32, 49]. In a recent work, by means of in situ time-resolved DRIFT spectroscopy, some of us observed, that CO species on gold sites with IR bands below 2100 cm⁻¹ (assigned to CO adsorbed on negatively charged gold clusters, Au^δ⁻) are the most reactive intermediates for the CO oxidation on a well-characterized Au/CeZrO₂ catalyst [30].

The results presented here for gold–iridium prove that extra catalytic sites, in addition to the usual active Au°–CO species (2110 cm⁻¹), are produced in the bimetallic Au–Ir/CeO₂ catalyst. These additional active sites could be produced and stabilized by the close interaction between gold
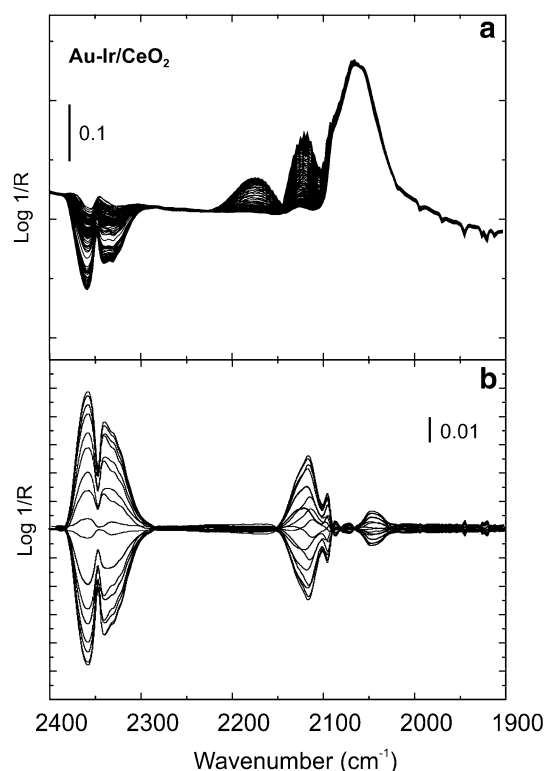
Fig. 9 a Time-domain DRIFT spectra during a c-MES cycle of CO(1 %) + O_2(1 %)/He switched to He over Au–Ir/CeO_2 (100 cm^3/min, 35 °C, ω = 8.33 mHz). **b** Phase-domain spectra after PSD demodulation

and iridium, thus explaining the enhanced activity and stability of the bimetallic system.

4 Conclusions

In comparison with the monometallic gold or iridium catalysts supported on ceria, the bimetallic Au–Ir/CeO_2 catalyst exhibited noticeable activity enhancement for CO oxidation, together with superior stability. The origin of the observed synergism was investigated by a combination of techniques. HRTEM images with nanoanalysis by X-EDS and XPS suggest intimate contact between both metals in the (nano)sized crystallites, which anchored the gold sites, enhancing the catalyst stability. In-situ DRIFT spectroscopy was used to characterize the adsorption sites for CO and their reactivity at 35 °C. By means of c-MES experiments it was shown that Au^0–CO species are reactive in the mono- and bimetallic gold catalyst, but also that new active sites ($Au^{\delta-}$) are produced when gold and iridium coexist thus increasing catalytic activity. Ir–CO species, on the other hand, proved to be unreactive.

We believe that the present work could be of value for strategies aim to design more active and stable gold catalyst by employing a second metal to produce isolated reactive gold sites.

References

1. Bond GC, Louis C, Thompson DT (2006) Catalysis by gold. Imperial College Press, London
2. Dobrosz-Gómez I, Kocemba I, Rynkowski J (2009) Catal Lett 128:297
3. del Río E, Blanco G, Collins SE, Haro M, Chen X, Delgado J, Calvino J, Bernal S (2011) Top Catal 54:931
4. Laguna OH, Romero Sarria F, Centeno MA, Odriozola JA (2010) J Catal 276:360
5. Cargnello M, Gentilini C, Montini T, Fonda E, Mehraeen S, Chi M, Herrera-Collado M, Browning ND, Polizzi S, Pasquato L, Fornasiero P (2010) Chem Mater 22:4335
6. Tibiletti D, Fonseca A, Burch R, Chen Y, Fisher J, Goguet A, Hardacre C, Hu P, Thompsett D (2005) J Phys Chem B 109:22553
7. Pilasombat R, Daly H, Goguet A, Breen J, Burch R, Hardacre C, Thompsett D (2012) Catal Today 180:131
8. Scire S, Liotta L (2012) Appl Catal B 125:222
9. Scire S, Riccobene P, Crisafulli C (2010) Appl Catal B 101:109
10. Delannoy L, Fajerwerg K, Lakshmanan P, Potvin C, Méthivier C, Louis C (2010) Appl Catal B Environ 94:117
11. Petrova P, Tabakova T, Munteanu G, Zanella R, Tsvetkov M, Ilieva L (2013) Catal Commun 36:84
12. Bokhimi X, Zanella R, Angeles-Chávez C (2010) J Phys Chem C 114:14101
13. Gomez-Cortés A, Díaz G, Zanella R, Ramírez H, Santiago P, Saniger J (2009) J Phys Chem C 113:9710
14. Okumura M, Akita T, Haruta M, Wang X, Kajikawa O, Okada O (2003) Appl Catal B 41:43
15. Akita T, Okumura M, Tanaka K, Tsubota S, Haruta M (2003) J Electron Microsc 52(2):119
16. Zhao J, Jun NI, Xu J, Xu J, Cen J, Li X (2014) Catal Commun 54:72
17. Zanella R, Louis C (2005) Catal Today 107–108:768–777
18. Aguirre A, Collins SE (2013) Catal Today 205:34
19. Baurecht D, Fringeli UP (2001) Rev Sci Instrum 72:3782
20. Vecchietti J, Collins SE, Delgado J, Małecka M, del Río E, Chen X, Bernal S, Bonivardi AL (2011) Top Catal 54:201
21. Kruse N, Chenakin S (2011) Appl Catal A 391:367
22. Radnik J, Mohr C, Claus P (2003) Phys Chem Chem Phys 5:172–177
23. Peuckert M (1984) Surf Sci 144:451
24. Hufner S, Wertheim GK (1975) Phys Rev B 11:678
25. Zhdan A, Boreskov GK, Boronin AI, Egelhoff WF, Weinberg WH (1976) Surf Sci 61:25
26. Lin W, Cheng H, He L, Yu Y, Zhao F (2013) J Catal 303:110
27. Fonseca GS, Machado G, Teixeira S, Fecher G, Morais J, Alves M, Dupont J (2006) J Colloid Interface Sci 301:193
28. Tabakova T, Boccuzzi F, Manzoli M, Sobczak JW, Idakiev V, Andreeva D (2006) Appl Catal A 298:127

29. Boccuzzi F, Chiorino A, Tsubota S, Haruta M (1996) J Phys Chem 100:3625
30. del Río E, Collins SE, Aguirre A, Chen X, Delgado JJ, Calvino JJ, Bernal S (2014) J Catal 316:210
31. Chen MS, Goodman DW (2004) Science 306:252
32. Yoon B, Haakkinen H, Landman U, Wörz AS, Antonietti JM, Abbet S, Juadai K, Heiz U (2005) Science 307:403
33. Worz AS, Heiz U, Cinquini F, Pacchioni G (2005) J Phys Chem B 109:18418
34. Chakarova K, Mihaylov M, Ivanova S, Centeno MA, Hadjiivanov K (2011) J Phys Chem C 115:21273
35. Daté M, Imai H, Tsubota S, Haruta M (2007) Catal Today 122:222
36. Alexeev O, Gates BC (1998) J Catal 176:310
37. Lyons KJ, Xie J, Mitchell WJ, Weinberg WH (1995) Surf Sci 325:85
38. Marinova TS, Chakarov DV (1989) Surf Sci 217:65
39. Kisters G, Chen JG, Lehwald S, Ibach H (1991) Surf Sci 245:65
40. Solymosi F, Novak E, Molnar A (1990) J Phys Chem 94:7250
41. Mihaylov M, Ivanova E, Thibault-Starzyk F, Daturi M, Dimitrov L, Hadjiivanov K (2006) J Phys Chem B 110:10383
42. Rojas H, Díaz G, Martínez J, Castañed L, Gómez-Cortés A, Arenas-Alatorre J (2012) J Mol Catal A 363:122
43. Cíes JM, el Río E, López-Haro M, Delgado JJ, Blanco G, Collins SE, Calvino J, Bernal S (2010) Angew Chem Int Ed 49:9744
44. Bourane A, Nawdali M, Bianchi D (2002) J Phys Chem B 106:2665
45. Green IX, Tang W, Neurock M, Yates JT (2011) Science 333:736
46. Green IX, Tang W, McEntee M, Neurock M, Yates JT (2012) J Am Chem Soc 134:12717
47. Chen M, Goodman DW (2006) Acc Chem Res 39:739
48. Chen MS, Goodman DW (2004) Science 306:5694
49. Henao JD, Caputo T, Yang JH, Kung MC, Kung HH (2006) J Phys Chem B 110:8689